Deposition of ^{13}C tracer and impurity elements on the divertor of Wendelstein 7-X

Tomi Vuoriheimo[1], Antti Hakola[2], Jari Likonen[2], Sebastijan Brezinsek[3], Timo Dittmar[3], Matej Mayer[4], Chandra Prakash Dhard[5], Dirk Naujoks[5], Filip Tuomisto[1], and the W7-X team[5§]

[1] Department of Physics, University of Helsinki, Helsinki, Finland
[2] VTT, Espoo, Finland
[3] Forschungszentrum Jülich GmbH, Jülich, Germany
[4] Max-Planck-Institut für Plasmaphysik, Garching, Germany
[5] Max-Planck-Institut für Plasmaphysik, Greifswald, Germany
[§]The W7-X Team are the co-authors mentioned in the paper, T. Klinger et al 2019 *Nucl. Fusion* **59** 112004

E-mail: tomi.vuoriheimo@helsinki.fi

Received xxxxxx
Accepted for publication xxxxxx
Published xxxxxx

Abstract

Carbon impurity transport and deposition were investigated in the Wendelstein 7-X stellarator by injecting isotopically labelled methane ($^{13}CH_4$) into the edge plasma during the last plasma operations of its Operational Phase (OP) 1.2B experimental campaign. ^{13}C deposition was measured by secondary ion mass spectrometry (SIMS) on three upper divertor tiles located on the opposite side of the vessel to the $^{13}CH_4$ inlet. The highest ^{13}C inventories were found as stripe-like patterns on both sides of the different strike lines. These high deposition areas were also analysed for their impurity contents and the depth profiles of the main elements in the layers. Layered deposition of different impurity elements such as Cr, Ni, Mo and B was found to reflect various events such as high metallic impurities during the OP1.2A and three boronizations carried out during OP1.2B.

Keywords: W7-X, carbon, impurity, deposition

1. Introduction

Impurities and their deposition on wall materials may induce several issues for the operation of fusion reactors. These include for example increased tritium retention on areas dominated by deposition of eroded material and impurities, flaking of the deposited layers and finally dust formation. The thermal and mechanical properties of the deposited layers may also differ greatly from those of the wall materials.

Impurity transport was studied in the Wendelstein 7-X (W7-X) stellarator by carrying out a ^{13}C seeding experiment. Such experiments have been used widely in fusion reactors [1–4]. A tracer isotope of carbon (^{13}C) was injected into the edge plasma as isotopically labelled methane ($^{13}CH_4$). This was performed in order to investigate impurity transport and deposition on the divertor tiles around the plasma-facing components of the vacuum vessel. As the first wall materials are mostly graphite covered by ^{12}C, using ^{13}C as tracer isotope allows us to investigate how carbon is transported and deposited in the vessel.

The ^{13}C injections were done during the last 30 shots of the operational phase (OP) 1.2B [5,6]. After OP1.2B several divertor tiles were taken out for measurements. We measured depth profiles of ^{13}C and also of various common impurities

from samples with high ^{13}C inventories. With these measurements the goal was to determine the composition and structure of the deposits. In addition, the depth profiles of elements of interest were extracted and the layered structure of the deposits and their connection to the operational history of W7-X were investigated.

Three upper divertor tiles from the half module (HM) 5u were obtained for measurements. HM 5u is nearly on the opposite side of the stellarator vessel in comparison to the $^{13}CH_4$ inlet on HM 3l as can be seen in Figure 1 (a). Same island intercepts the horizontal part of both these divertors [7]. This way, the long-range migration of carbon and other impurities in W7-X could be assessed. The locations of the three tiles on the divertor island are shown in Figure 1 (b).

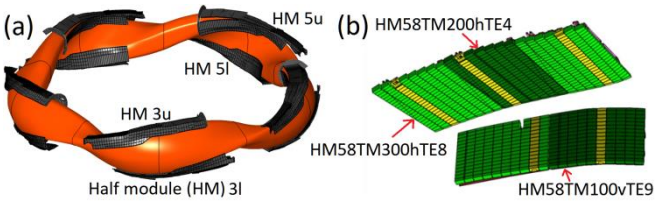

Figure 1: (a) CAD drawing of the divertor islands. The measured tiles were on HM 5u and the ^{13}C inlet on HM 3l. Figure adapted from [8]**. (b) The three tiles analyzed on the horizontal and vertical divertor tiles on the 5u divertor island.**

2. Experimental

2.1 Sample preparation

Cylindrical samples with a diameter of 17 mm were drilled from the three tiles received for measurements. Samples were taken close to each other to ensure that all the areas of interest would be analyzed. One or two samples were drilled in the toroidal direction based on the visual appearance of the tile surface. A photo of the tile after the sample extraction can be seen in Figure 2.

Figure 2: Tile HM58TM200hTE4 after drilling of samples

2.2 Secondary ion mass spectrometry

The amount of ^{13}C and other impurities as well as their depth profiles were measured using secondary ion mass spectrometry (SIMS) at the VTT facilities in Espoo, Finland. Here we used 5 keV O_2^+ primary ions with a current of 500 nA. This resulted in a sputtering rate of 1-2 nm/s on the graphite tiles. The exact rate depended on the depositions on the tile surface: thick impurity-rich deposits were sputtered faster than the graphite substrate.

The sputtered craters were up to 7 µm deep. A stylus profilometer (Dektak 3ST) was applied to calibrate the measurement time versus the crater depth. The primary ion beam was rastered across an area of 0.3×0.4 mm^2. A 10% electronic gate and a 1 mm optical gate were used in all the measurements to eliminate the disturbing ejection of particles from the edges of the SIMS crater.

With SIMS we measured the depth profiles of 8 mass signals. Each mass cycle was about 12 seconds with the signal averaged over 1.5 seconds. This gives us a depth resolution of 10-20 nm.

The ^{13}C profiles were measured with a high mass resolution ($m/\Delta_m \approx 2000$) to separate ^{13}C from closely lying isobars such as ^{12}CH. There was still some overlap which caused the background to be about 1.2%, slightly higher than the expected natural background of 1.1%. The background level of ^{13}C was subtracted from the data. The mass signals of ^{13}C were integrated over the depth profiles to calculate the concentrations. The signal for ^{13}C was calibrated using a reference layer with a known concentration of ^{13}C.

Other impurities were measured afterwards from the samples with thick ^{13}C depositions. During these measurements we used a lower mass resolution ($m/\Delta_m \approx 300$) to obtain higher signal strengths for all the impurities. Because of this ^{13}C and ^{12}CH were somewhat overlapping on the mass 13 signal. The elements we measured were H, B, ^{12}C, ^{13}C with ^{12}CH, Na, Cr, Ni and Mo. In addition Fe was also measured on a few samples but the shape of the depth profile was found to be similar to that of Cr.

3. Results and discussion

3.1 ^{13}C deposition profiles

The SIMS depth profile data were integrated over the depth, giving the total amount of ^{13}C for each measurement point. The measurements were repeated at three poloidal locations with a distance of about 4 mm between successive points.

Results for the vertical divertor tile HM58TM100vTE9 can be seen in Figure 3 and for the horizontal divertor tiles HM58TM200hTE4 and HM58TM300hTE8 in Figure 4 and Figure 5 respectively. T1 and T2 represent the samples in the toroidal direction and can be seen in Figure 2.

On tile HM58TM100vTE9 shown in Figure 3, a high deposition area with ^{13}C surface densities up to 3×10^{17} $^{13}C/cm^2$ is observed at a distance of around 100 mm from the pumping gap. Throughout the remaining areas of the tile surface there is also deposition of about 1×10^{17} $^{13}C/cm^2$ on most of the tile and only one area with very little deposition around 200 mm from the pumping gap. Differences between the T1 and T2 samples are very small which implies that the deposits are formed as stripe-like

patterns in the toroidal direction. This is also suggested by the visual impression of the tiles.

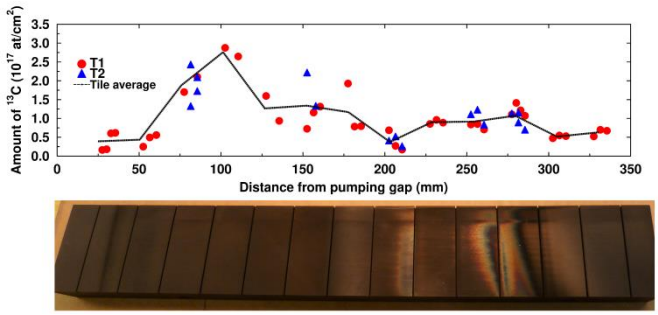

Figure 3: Vertical divertor tile HM58TM100vTE9 and its ^{13}C deposition

In Figure 4 there are two low deposition areas that have been earlier associated with strike lines areas and thus zones with a considerable erosion [9]. Erosion from these areas causes high redeposition to nearby regions. The peak values here are slightly lower than in Figure 3, around 2×10^{17} ^{13}C/cm^2. In the toroidal direction the differences are again small, and mainly reflecting the direction of the deposition bands being tilted with respect to the toroidal direction.

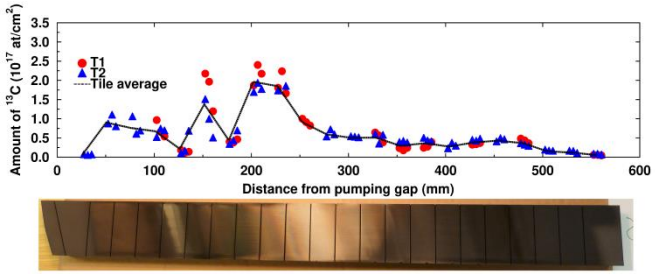

Figure 4: Horizontal divertor tile HM58TM200hTE4 and its ^{13}C deposition

The results extracted from another horizontal divertor tile are presented in Figure 5. The strike line around 150 mm from the pumping gap is broad and there is considerable deposition up to 3×10^{17} ^{13}C/cm^2 on both sides of it. The total amount of deposited ^{13}C is about the same near the strike lines on Figure 4 and Figure 5. Due to the differences in the strike lines the exact positions of the deposition maxima are different.

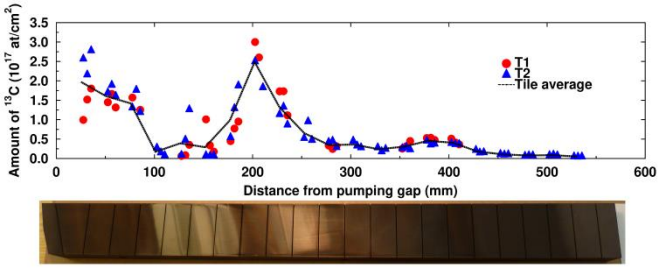

Figure 5: Horizontal divertor tile HM58TM300hTE8 and its ^{13}C deposition

3.2 Depth profiling of other impurities

As discussed in section 2, depth profiles of the selected impurities other than ^{13}C were measured with the lower mass resolution. As the yields of different elements other than ^{13}C were not calibrated, we can only see the relative changes in their depth profiles. Therefore quantification is not possible but data from the different samples can be compared with each other. This is due to the different sensitivity and sputtering ratios for the different elements.

In most of the low impurity data outside of the highest deposition areas, most of the impurity signals exhibited their maxima on the surface. In these cases the overall deposition on the tiles is relatively low. An example of depth profiles measured from one of these samples is presented in Figure 6 (a). The impurity levels are generally the highest on the surface and then gradually decrease deeper into the sample, especially beyond 1-2 µm. The exception is boron where a secondary peak is visible at a depth of 1-1.5 µm.

In Figure 6 (b) we can see more complex impurity depth profiles. This sample is located close to the strike lines which has caused high deposition of impurities nearby. Boronizations were done three times during OP1.2B in W7-X [10,11] so we can assume that the boron-rich layer in a depth around 0.5-2 µm was formed during these events. We can see high impurity levels for Cr, Ni and Mo deeper than 2 µm in the sample. These can be associated with the high impurity levels seen during OP1.2A [11–13]. Complementary information about the impurities can be found in [14]. Closer inspection of the depth profiles allows reconstructing the timeline of the various plasma experiments during OP1.2. The discussion on this is left for a future publication.

Another example of the complex impurity layers can be seen in Figure 6 (c). There is again a distinct layer of boron representing the three boronizations. The boron signal is much higher in Figure 6 (b) than Figure 6 (c): the sample used in Figure 6 (b) was next to the broad strike line and had a higher maximum for ^{13}C as well. The two separate strike lines for the sample in Figure 6 (c) might have affected the difference in the boron levels.

W7-X has 71.4 m^2 of plasma-facing components made of stainless steel (SS), these are namely; wall panels (57.8 m^2), poloidal divertor closures (8.1 m^2) and pumping gap panels (5.5 m^2). The Cr, Ni and Mo impurities are expected to be originated from these SS components due to the sputtering due to charge-exchange process during plasma operation and glow discharge cleaning in He and boronizations. Since these impurities appear together with B (until the depths up to 5000 nm) which was injected during OP1.2B, these depositions have most likely occurred during OP1.2B. The Na impurity might have originated from

alkali-beam diagnostics [15] that used sodium during OP1.2A.

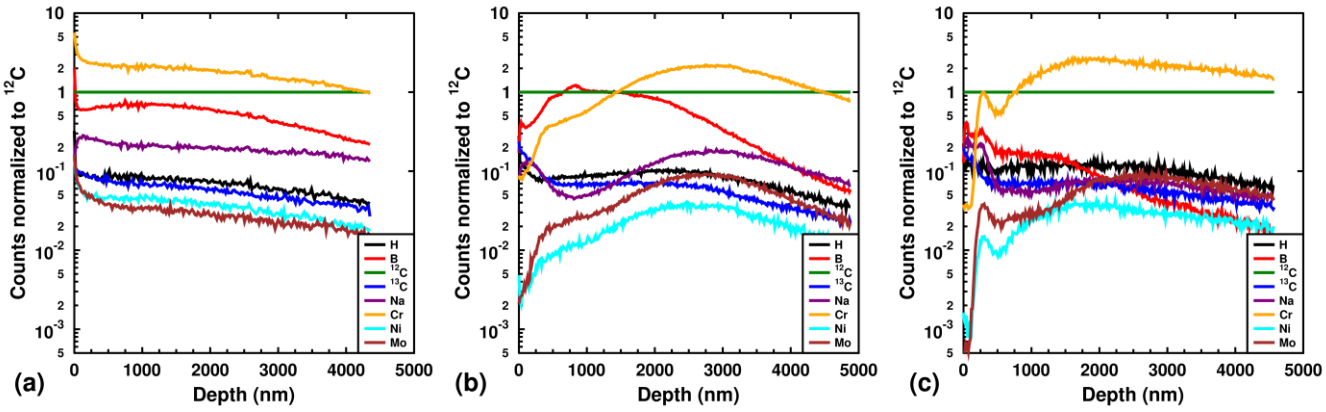

Figure 6: SIMS depth profile of impurities measured from (a) HM58TM100vTE9P3T2, (b) HM58TM300hTE8P8T2 and (c) HM58TM200hTE4P8T1. In (a) most of the impurity maxima are on the surface and there are no other clear layers deeper aside from boron. In (b) and (c) there are several maxima for many impurities suggesting complex impurity layers in the deposition areas.

4. Conclusions

From the ^{13}C deposition results it is clear that the impurity depositions have high local variation. The thickest deposits are measured next to the strike lines with the most noticeable erosion. A similar effect has been observed also by numerically modelling the experiment [6].

Metallic impurities and boron were observed to form complex layers on the deposition-dominated areas. This information can be used to investigate the impurity content in the fusion device during different times of the operation. Boronizations affected the impurity deposition depth profiles significantly by reducing the common metallic impurities.

Our samples were all from the same divertor island in the W7-X. Measuring and comparing tiles from different areas after the upcoming operational phases will also tell us more about the local conditions in the vessel. This is a topic of our future work.

Acknowledgements

This work has been carried out within the framework of the EUROfusion Consortium and has received funding from the Euratom research and training programme 2014-2018 and 2019-2020 under grant agreement No 633053. The views and opinions expressed herein do not necessarily reflect those of the European Commission.

References

[1] Wienhold P, Esser H G, Hildebrandt D, et al 2001 *J. Nucl. Mater.* **290**–**293** 362
[2] Vainonen-Ahlgren E, Likonen J, Renvall T, et al 2005 *J. Nucl. Mater.* **337**–**339** 55–9
[3] Likonen J, Airila M, Alves E, et al 2011 *Phys. Scr.* **T145** 014004
[4] Möller S, Ding R, Xie H, et al 2020 *Nucl. Mater. Energy* **25** 100805
[5] Brezinsek S et al. Presented at IAEA FEC 2021 / submitted to *Nucl. Fusion*
[6] Schmid K, Effenberg F, Dinklage A, et al 2020 *Nucl. Mater. Energy* **25** 100821
[7] Endler M, Baldzuhn J, Beidler C D, et al 2021 *Fusion Eng. Des.* **167** 112381
[8] Pedersen T S, König R, Krychowiak M, et al 2018 *Plasma Phys. Control. Fusion* **61** 14035
[9] Mayer M, Balden M, Brezinsek S, et al 2020 *Phys. Scr.* **T171** 14035
[10] Fuchert G, Brunner K J, Rahbarnia K, et al 2020 *Nucl. Fusion* **60** 036020
[11] Sereda S, Brezinsek S, Wang E, et al 2020 *Nucl. Fusion* **60** 86007
[12] Wang E, Brezinsek S, Sereda S, et al 2020 *Phys. Scr.* **T171** 14040
[13] Klinger T, Andreeva T, Bozhenkov S, et al 2019 *Nucl. Fusion* **59** 112004
[14] Zhao D, Yi R, Oelmann J, et al 2020 *Phys. Scr.* **T171** 014018
[15] Zoletnik S, Anda G, Aradi M, et al 2018 *Rev. Sci. Instrum.* **89** 10D107